Redox Biology 28 (2020) 101328

Contents lists available at ScienceDirect

Redox Biology

journal homepage: www.elsevier.com/locate/redox

Research Paper

Insight into the mechanism of ferroptosis inhibition by ferrostatin-1

Giovanni Miotto[a,b,1], Monica Rossetto[a,1], Maria Luisa Di Paolo[a], Laura Orian[c], Rina Venerando[a], Antonella Roveri[a], Ana-Marija Vučković[a], Valentina Bosello Travain[a], Mattia Zaccarin[a], Lucio Zennaro[a], Matilde Maiorino[a], Stefano Toppo[a,b], Fulvio Ursini[a,**], Giorgio Cozza[a,*]

[a] Dept. of Molecular Medicine, University of Padova, V.le G. Colombo, 3, I-35121, Padova, Italy
[b] CRIBI Biotechnology Center, University of Padova, V.le G. Colombo, 3, I-35121, Padova, Italy
[c] Dept. of Chemical Sciences, University of Padova, Via Marzolo, 1, I-35131, Padova, Italy

ARTICLE INFO

Keywords:
Ferroptosis
Ferrostatin-1
Antioxidant
Lipid peroxidation
GPx4
Alkoxyl radical

ABSTRACT

Ferroptosis is a form of cell death primed by iron and lipid hydroperoxides and prevented by GPx4. Ferrostatin-1 (fer-1) inhibits ferroptosis much more efficiently than phenolic antioxidants. Previous studies on the antioxidant efficiency of fer-1 adopted kinetic tests where a diazo compound generates the hydroperoxyl radical scavenged by the antioxidant. However, this reaction, accounting for a chain breaking effect, is only minimally useful for the description of the inhibition of ferrous iron and lipid hydroperoxide dependent peroxidation. Scavenging lipid hydroperoxyl radicals, indeed, generates lipid hydroperoxides from which ferrous iron initiates a new peroxidative chain reaction. We show that when fer-1 inhibits peroxidation, initiated by iron and traces of lipid hydroperoxides in liposomes, the pattern of oxidized species produced from traces of pre-existing hydroperoxides is practically identical to that observed following exhaustive peroxidation in the absence of the antioxidant. This supported the notion that the *anti*-ferroptotic activity of fer-1 is actually due to the scavenging of initiating alkoxyl radicals produced, together with other rearrangement products, by ferrous iron from lipid hydroperoxides. Notably, fer-1 is not consumed while inhibiting iron dependent lipid peroxidation. The emerging concept is that it is ferrous iron itself that reduces fer-1 radical. This was supported by electroanalytical evidence that fer-1 forms a complex with iron and further confirmed in cells by fluorescence of calcein, indicating a decrease of labile iron in the presence of fer-1. The notion of such as pseudo-catalytic cycle of the ferrostatin-iron complex was also investigated by means of quantum mechanics calculations, which confirmed the reduction of an alkoxyl radical model by fer-1 and the reduction of fer-1 radical by ferrous iron. In summary, GPx4 and fer-1 in the presence of ferrous iron, produces, by distinct mechanism, the most relevant *anti*-ferroptotic effect, *i.e* the disappearance of initiating lipid hydroperoxides.

1. Introduction

Ferroptosis (FPT) is a recently described non-apoptotic form of regulated cell death (RCD) [1], first disclosed as a suitable target for anti-cancer therapy. Ferroptosis was later identified as the mechanism of cell death in major neurodegenerative diseases, including Parkinson and Huntington disease [2], cerebello-cortical atrophy and post-traumatic cerebral injury [3,4], as well as sepsis [5], bacterial [6] and viral diseases [7]. The common motif is missing activity of the selenoperoxidase GPx4 resulting in activation of lipid peroxidation [8]. The death phenotype of GPx4 knock-out, indeed, is reproduced in experimental and spontaneous diseases and is rescued by: i) chelating iron; ii)

Abbreviations: FTP, Ferroptosis; GPx4, Glutathione Peroxidase 4; RCD, regulated cell death; LPO, lipid peroxidation; GSH, glutathione; fer-1, ferrostatin-1; ABIP, 2,2′-azobis[2-(2-imidazolin-2-yl)propane]; SLPC, 1-stearolyl-2-lineoyl-*sn* glycero-3-phosphocholine; SLPE, 1-stearolyl-2-lineoyl-*sn*-glycero-3-phosphoethanolamine; PLPC, 1-palmitoly-linoleoyl-*sn*- glycero-3-phosphocholine; PLPE, 1-palmitoly-linoleoyl-*sn*-glycero-3-phosphoethanolamine; MRBE, Methyl *tert*-butyl ether; LIP, Labile Iron Pool; DFT, density functional theory; HAT, hydrogen atom transfer; MFI, mean fluorescence intensity; PL-OOH, phospholipid hydroperoxides; PL-OH, phospholipid alcohol; PL, phospholipid containing polyunsaturated fatty acid; PL$^{\bullet}$, phospholipid carbon centered radical; PL-OO$^{\bullet}$, phospholipid hydroperoxyl radical; PL-O$^{\bullet}$, phospholipid alkoxyl radical

* Corresponding author.
** Corresponding author.
E-mail addresses: fulvio.ursini@unipd.it (F. Ursini), giorgio.cozza@unipd.it (G. Cozza).
[1] The two authors equally contributed to this work.

https://doi.org/10.1016/j.redox.2019.101328
Received 23 July 2019; Received in revised form 5 September 2019; Accepted 15 September 2019
Available online 20 September 2019

decreasing unsaturation of fatty acid of phospholipids; iii) free radical scavenging [8].

FPT can be defined, therefore, as an RCD operated by lipid peroxidation (LPO), which can only proceed when the enzymatic reduction of phospholipid hydroperoxides (PL-OOH) is missing or deeply limited, in respect to the rate of their formation [8].

The mechanism of LPO leading to FPT is *bona fide* fully overlapping that of iron dependent microsomal lipid peroxidation, described more than half a century ago, and that, incidentally, drove to the discovery of GPx4 as a unique and peculiar "peroxidation inhibiting protein", the *anti*-peroxidant activity of which cannot be substituted by any other antioxidant enzyme [9,10]. Membrane LPO is the oxidative degradation of poly-unsaturated phospholipid primed by ferrous iron complexes and pre-existing lipid hydroperoxides [9–11]. Therefore, the unique enzymatic reaction competent for preventing the whole peroxidative event is the reduction of PL-OOH by GPx4 using GSH as reducing substrate [8]. In other words, it is the effect of GPx4 that provides the non-ambiguous evidence that LPO is initiated from PL-OOH. Although this could appear counterintuitive, being PL-OOH the product of LPO, the conundrum is solved having in mind that traces of PL-OOH can be formed independently from the initiation and progression of fast peroxidative chain reactions [12]. In the absence of specific challenges, GPx4 and GSH keep catalyzing the reduction of PL-OOH, which are produced at trace level amounts during aerobic metabolism, into corresponding phospholipid alcohols (PL-OH). Notably, PL-OOH can be also produced by lipoxygenases [13], with special reference to 12/15-lipoxygenase (ALOX-12/15), and this seems also relevant to FPT [14]. However, also the activity of this lipoxygenase requires activating lipid hydroperoxides and is, therefore, under the control of GPx4 activity [15].

LPO of biological membranes encompasses free radical reactions summarized as: i) initiation, beginning with the abstraction by the initiating free radical of a hydrogen atom from a phospholipid containing polyunsaturated fatty acid (PL), leading to a phospholipid carbon centered radical ($PL^{\bullet}$), and proceeding with the oxygen addition to the $PL^{\bullet}$ (hydroperoxyl radical, $PL\text{-}OO^{\bullet}$) [16]; ii) chain propagation, through the reaction between $PL\text{-}OO^{\bullet}$ and another PL, resulting in a phospholipid hydroperoxide (PL-OOH); and iii) arrest, by scavenging or radical-radical interactions [17].

In the frame of this simplified scheme of process, LPO is initiated by Fe^{2+} from PL-OOH. The weak O–O bond of PL-OOH is indeed easily cleaved by Fe^{2+}, producing the extremely reactive alkoxyl radical ($PL\text{-}O^{\bullet}$) competent for initiation [16]. Thus, $PL\text{-}O^{\bullet}$ is involved in the initiation of LPO, while $PL\text{-}OO^{\bullet}$ is driving propagation [18].

Mechanistic and kinetic studies on LPO, in the last decades, largely took advantage of the use of azo initiators introduced by Keith Ingold [19]. By thermal decomposition, in a first-order reaction, these species produced a carbon centered radical evolving to a hydroperoxyl radical in the diffusion limited reaction with oxygen [19,20]. This kinetic approach permitted the careful evaluation of the "antioxidant capacity" of compounds, or even heterogeneous mixtures, in terms of apparent rate constant for scavenging hydroperoxyl radicals, usually having as a reference tocopherol, the paradigmatic antioxidant [21]. Notably, in this kinetic assay, it is the propagating hydroperoxyl radical that actually initiates LPO. For this reason, the information achieved from using azo compounds is limited to the "chain breaking" efficiency of the antioxidant under scrutiny. The specificity of this concept is often overlooked in scientific literature when the notion of "chain breaking antioxidant" is considered fully overlapping the concept of "free radical scavenging antioxidant". This could be of not trivial relevance when dealing with iron dependent LPO, since reducing $PL\text{-}OO^{\bullet}$ generates PL-OOH from which Fe^{2+} keeps regenerating initiating radicals, by Fenton like reaction.

By high-throughput screening of small molecule libraries, it was independently reported that fer-1 [1] and liproxstatin-1 (lip-1) [22] act as potent inhibitors of ferroptosis, [22,23]. Unexpectedly, α-tocopherol (α-TOH) emerges as a relatively weak inhibitor of ferroptosis when compared to either fer-1 or lip-1 [22–24].

In this study, we addressed the mechanism of fer-1 in a model system of LPO, more representative of the biochemical events leading to FPT.

2. Materials and methods

2.1. Reagents

Phospholipids: 1-stearoyl-2-linoleoyl-*sn*-glycero-3-phosphocoline (18:0–18:2 PC, SLPC) and 1-stearoyl-2-linoleoyl-*sn*-glycero-3-phosphoethanolamine (18:0–18:2 PE, SLPE) were from Avanti Polar Lipids, USA. Tris, trolox, ferrostatin (fer-1), ascorbic acid, $FeSO_4$, glutathione and hexane (mass-spectrometry grade) and Methyl *tert*-butyl ether (MTBE) were from Sigma. Deferasirox from Santa Cruz and calcein-AM from Thermo Fisher. Acetonitrile, Isopropanol from VWR. 2,2′-azobis [2-(2-imidazolin-2-yl)propane] (ABIP) was a kind gift of Wako Chemicals (Neuss, Germany). GPx4 was purified from rat testis [25]. Expression vectors containing human ALOX15 sequence was a kind gift from H. Kuhun (Institute of Biochemistry, University Medicine Berlin-Charité, Charitéplatz 1, D-10117 Berlin, Germany) and the recombinant protein was obtained according to Ref. [26].

2.2. Liposome preparation

Chloroform solution of SLPC and SLPE (10 mg/mL) were mixed in equimolar ratio in a glass tube. After chloroform has been removed by nitrogen flux, the dried phospholipids mixture was suspended with buffer (0.1 M Tris, 0.15 M NaCl, pH 7.4) in order to obtain a final total lipids concentration of 0.1 mM and then vortexed for 2 min. A homogeneous population of unilamellar liposomes were finally obtained by extruding 10 times the lipids suspensions through 0.1 μm polycarbonate filters (Whatman Nuclepore Track Etched Membranes), using an extruder (LIPEX^{R} Extruder Transferra Nanosciences Inc. Canada) at 50 °C [27].

2.3. Inhibition of Liposome peroxidation

Liposome solution was introduced in oxygraphic cell (volume 1.5 mL) and equilibrated with air at 37.0 ± 0.1 °C. After thermal equilibration, 5 μL of inhibitor in ethanol (fer-1 or trolox) were added and after 1 min peroxidation was started by adding either: i) 24 μL of 0.5 M ABIP in water, a diazo compound which thermally decomposes producing a constant source of peroxyl radicals (K_d 2.44 × 10^{-4} min^{-1}); or ii) iron and ascorbic acid. 5 μL fresh solution of 9 mM ascorbic acid in water and 5 μL of 1.2 mM $FeSO_4$ in 10 mM HCl were used, unless otherwise indicated. The rate of oxygen consumption was measured in the absence (R_0) and in the presence (R) of inhibitor and IC_{50} was calculated as previously described [28,29].

$$R/R_0 = K + (1\text{-}K)e^{-\ln 2 \cdot C/IC_{50}} \quad (1)$$

where K is a constant corresponding to the relative rate of O_2 consumption extrapolated at high inhibitor concentration, C the inhibitor concentration, IC_{50} is the inhibitor concentration required to decrease the ratio R/R_0 from 1 to K + (1-K)/e. In the case of the oxidation induced by ABIP the stoichiometry n, representing the amount of peroxyl radicals trapped by the inhibitor, was calculated according to the equation n = R_i x LT/C, where LT is the lag time of inhibition, R_i the initiation rate. The oxygen consumption rate was followed by a Yellow Springs oxygen electrode using a Metrohm 663 VA potentiostat in a thermostatted oxygraphic cell.

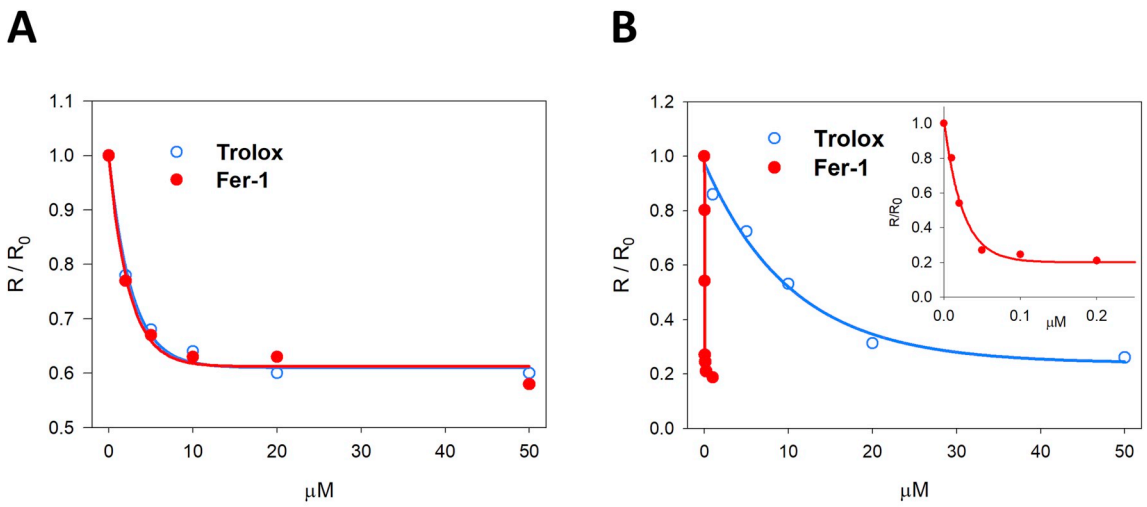

C

	ABIP		Fe^{2+}/Ascorbate
	n	IC_{50} (μM)	IC_{50} (μM)
Trolox	2	1.86	7.2
Fer-1	4.16	1.66	0.017

Fig. 1. Inhibition of lipid peroxidation induced with iron or diazo in liposome. The dependence of initial oxygen consumption rate ratio R/R_0 from trolox (blue open circle) and fer-1 (red full circle, also expanded into the inset) concentration was fitted to Eq (1) (See Materials and Methods). Liposome solution containing 0.1 mM phospholipids (SLPC:SLPE/1:1), different amount of trolox or fer-1 was oxidized by 8 mM ABIP (panel A) or 30 μM ascorbic acid and 4 μM $FeSO_4$ (panel B) in 0.1 M Tris, 0.15 M KCl at pH 7.0, at 37 °C. In (C) IC_{50} values calculated from panels A and B are reported. (For interpretation of the references to colour in this figure legend, the reader is referred to the Web version of this article.)

2.4. One phase lipid extraction (OPE) of liposomes

50 μl of liposomes suspension was mixed with 1 ml of OPE mixture: methanol:MTBE:chloroform - 1.33:1:1 v/v/v. Thus, the tubes were covered, vortexed for 30 s, and shaken for 20 min at 1000 rpm at room temperature. Next, the tubes were centrifuged 5 min at 12000 g, room temperature, then diluted 1:2 with initial mobile phase (68% A: 32% B) and an aliquot of 0.2 μl subjected to LC/MS analysis.

2.5. LC - MS/MS analysis

Samples were analyzed by LC-MS/MS using a 6520 Q-TOF mass spectrometer governed by Agilent MassHunter software (B.05.00 version), coupled on-line with a 1200 series HPLC system through a Chip Cube nano-ESI interface (Agilent Technologies, CA, USA). Chromatographic separations were performed on a reverse phase, high resolution 3 μm C18 Polaris chip-column (Polaris-HR-3C18, Agilent Technologies), integrating a 360 nL capacity trap-column, the column (0,75 mm × 150 mm), connection capillaries, and a nano-spray emitter.

2.5.1. Phospholipids analysis by LC/MS

0.2 μl of sample, extracted as described above, were chromatographically separated according to Pellegrino et al. [30] with minor modifications. In brief, the mobile phases was A: 5 mM ammonium formate in water/acetonitrile/methanol: 40/50/10, B: 5 mM ammonium formate in isopropanol/acetonitrile/hexane: 90/10/10. The gradient was as follows: 0–1 min solvent A from 68% to 49%; 1–15 min A from 49% to 4%; hold for 7 min and then let to re-equilibrate for 18 min at initial conditions; the flow was 0.35 μL min^{-1}.

The Q-TOF operates in MS mode at 2 GHz extended dynamic range, with three reference ions. Capillary voltage was set to 1350 V (negative polarity) with nitrogen as desolvating gas at 330 °C and 4.8 l/min; fragmentor, skimmer, and octapole were set at 150, 65, and 750 V, respectively.

Mass spectra were acquired in a data dependent mode: MS/MS spectra of the 7 most intense ions were acquired for each MS scan in the 100–1700 Da range. Scan speed was set to 2 MS spectra s-1 and 3 MS/MS spectra s-1 (see Supplementary Material).

2.5.2. Lipids identification and quantification

Identification of oxidized lipids was performed by fragmentation pattern (MS/MS) and retention time (see Supplementary Material). Due to the nature of the phospholipids forming the liposomes, only the MS/MS spectra containing the fragments relative to stearoyl moiety [283.26]- and the polar head of phosphatidyl-ethanolamine [140.01]- or phosphatidyl-choline [168.04]- were considered. The screening of MS/MS spectra was carried out both manually and by a dedicated function for oxidized lipids identification implemented in LIPOSTAR, a software recently developed by Cruciani's group [31]. Both approaches lead to the identification of the same pattern of oxidized species from either 1-stearoyl-2-linoleoyl-*sn*-glycero-3-phosphocoline (SLPC) or 1-stearoyl-2-linoleoyl-*sn*-glycero-3-phosphoethanolamine (SLPE). The detection limits, calculated by calibrated deuterate standards (PC(15:0/18:1(d7)); PE (15:0/18:1(d7)), Avanti Polar Lipids), were 0.6 and 0.4 injected fmoles for SLPC and SLPE respectively, corresponding to about 1/1000 of total amount of injected phospholipids. Due to the lack of

Table 1
Oxidized species of SLPC identified by oxi-lipidomic. All species have been generated from linoleic acid. The same species have been detected in PLPC, SLPC and PLPE. Identification was obtained by retention time and MS/MS.

Oxidized species	Acronym	Structure R = $C_8H_{15}O_2$	*m/z*
1[O] epoxy	1[O](epoxy)	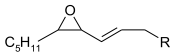	296.2351
1[O] hydroxy	1[O]	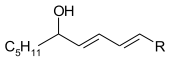	296.2351
1[O](-H2) keto	1[O](-H2)	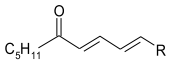	294.2195
2[O] hydroperoxy	2[O](Hp)	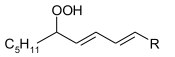	312.2301
2[O] epoxy-hydroxy	2[O]	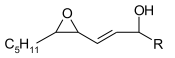	312.2301
2[O](-H2) epoxy-keto	2[O](-H2)	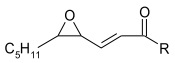	310.2144
3[O] hydroperoxy-epoxy	3[O](Hp)	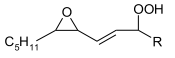	328.225
3[O] epoxy-hydroxy	3[O]	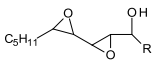	328.225
3[O](-H2) keto - epoxy	3[O](-H2)	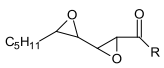	326.2093

Truncated species	Acronym	Structure R = H	m/z
9-oxo-nonanoyl		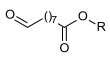	172.1099
azelaoyl		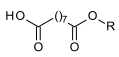	188.1049
8-oxo-octanoyl		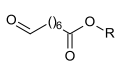	158.0943
8-OH-octanoyl		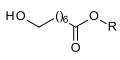	160,1099

oxidized lipids standards, the ionization yields of oxidized species was assumed equal to their precursor (SLPC and SLPE). Minimal differences, due to liposome preparations, have been minimized expressing the amount of each oxidized species as a percentage of the total (precursor plus oxidized).

2.5.3. Ferrostatin analysis by LC/MS

Liposomes suspension was extracted as above, then 200 µL were dried under vacuum (Speedvac), and dissolved in 100 µl of 33% aqueous acetonitrile.

Each sample (0.8 µL) underwent 10 min isocratic separation, the mobile phases consisted of acetonitrile/water: 90/10, containing 0.1% formic acid. The flow was maintained at 0.3 µL min-1.

The Q-TOF operates in MS mode at 2 GHz extended dynamic range, with three reference ions. Capillary voltage was set to 1600 V (positive polarity) with nitrogen as desolvating gas at 325 °C and 4.8 L/min; fragmentor, skimmer, and octapole were set at 140, 65, and 750 V, respectively.

Mass spectra were acquired in a data dependent mode: MS/MS spectra of the 6 most intense ions were acquired for each MS scan in the 100–1700 Da range. Scan speed was set to 2 MS spectra s^{-1} and 3 MS/MS spectra s^{-1}.

Ferrostatin was identified by exact mass [263.175] + and by the fragmentation pattern of the standard (see Supplementary Material). The detection limit was 1 injected femtomole.

2.6. Computational details

All the density functional theory (DFT) calculations were performed using Gaussian16 [32]. Full geometry optimizations were in gas-phase using M06-L functional [33] combined with 6-31G(d,p) basis set for all the atoms, except Fe for which LanL2DZ was used with an effective core potential. Unrestricted open-shell formalism was adopted for all the species with unpaired electrons; thus, spin contamination was checked to assess the reliability of the wavefunction. Frequency calculations were carried out at the same level of theory (M06-L/6-311 + G(d,p),Lanl2DZ) in order to confirm the stationary points (all positive frequencies). Afterwards, single point energy calculations were performed at SMD-M06-L/6-311 + G(d,p),LanL2DZ//M06-L/6-31G(d,p),LanL2DZ in gas phase in order to obtain more accurate energy values, and subsequently, at the same level of theory, in benzene and water using the SMD continuum model [34]. This level of theory, denoted SMD-M06-L/6-311 + G(d,p)//M06-L/6-31G(d,p), allows to estimate free energies in condensed phase and benzene and water were chosen to mimic an apolar and a polar environment, respectively [35]. Cartesian coordinates of the optimized molecular structures are reported in Supplementary Material.

2.7. Electrochemical methods

Differential pulse voltammetry (DPV) experiments were carried out by using an Autolab PGSTAT connected to a three-electrode strip sensor (G-Sensor from the Ecobioservice & Researches s.r.l., Firenze, Italy) and in a 700 µL micro cell. The electrodes on the G-Sensor were: a glassy carbon electrode of 3 mm of diameter (as working electrode), Ag (as pseudo-reference electrode) and carbon (as counter electrode). This strip sensor was chosen because fer-1 was easily adsorbed to glassy carbon electrodes (as reported also for other redox compounds [36,37]) and consequently the use of these strips allowed the renewal of the surface of working electrode (without polishing the electrode surface).

DPV experiments were carried out at 25 °C with following set-up: scan rate 10 mVs^{-1}, step potential 50 mV, modulation amplitude 20 mV, modulation time 0.07 ms and interval time was 200 ms. Scan potential was from -800 to +1000 mV. The stock solution of $FeSO_4$ was 5 mM in 10 mM HCl, and $FeCl_3$ was 10 mM in 25 mM HCl. Fer-1 stock solution was 40 mM in DMSO. The medium of the electrochemical experiments was MetOH 90%, 0.1 M $LiClO_4$ (as supporting electrolyte). Other buffers were tested, such as Tris/HCl 0.1 M, KCl 0.15 M pH 6.8 in absence and presence of 25% methanol, but a significant adsorption on electrode surface was found. No significant signal of Fe^{2+} or Fe^{3+} (at maxima concentration 160 µM) or of the HCl solution were found on the DPV of the blank solution (in absence of fer-1) and in the potential range explored for fer-1. Analysis of data was performed with Sigma Plot 9.0 software, Jandel Scientific, San Rafael, CA USA.

2.8. Measurement of the cellular Labile Iron Pool (LIP)

Sub-confluent HEK293T cells, seeded the day before, were incubated for 210 min in DMEM, without FBS, with increasing concentration of ferrostatin-1. Calcein-AM 50 nM, was added 45 min before the end of the incubation. After trypsinization, cells were suspended in phosphate buffer solution (PBS) and rapidly analyzed by flow cytometry (BD-FACSCanto II, equipped with a 488 nm argon laser). The emission of 20000 cells was recorded at 530 nm and the mean fluorescence intensity (MFI) was calculated by FACS DIVA software (Becton-Dickinson). The relative LIP was expressed as percentage of calcein-MFI of cells treated vs control. Cells incubated with Deferasirox 100 µM served as baseline. The values are the mean ± standard deviation (SD) of 2 independent experiments in triplicate (GraphPad Prism).

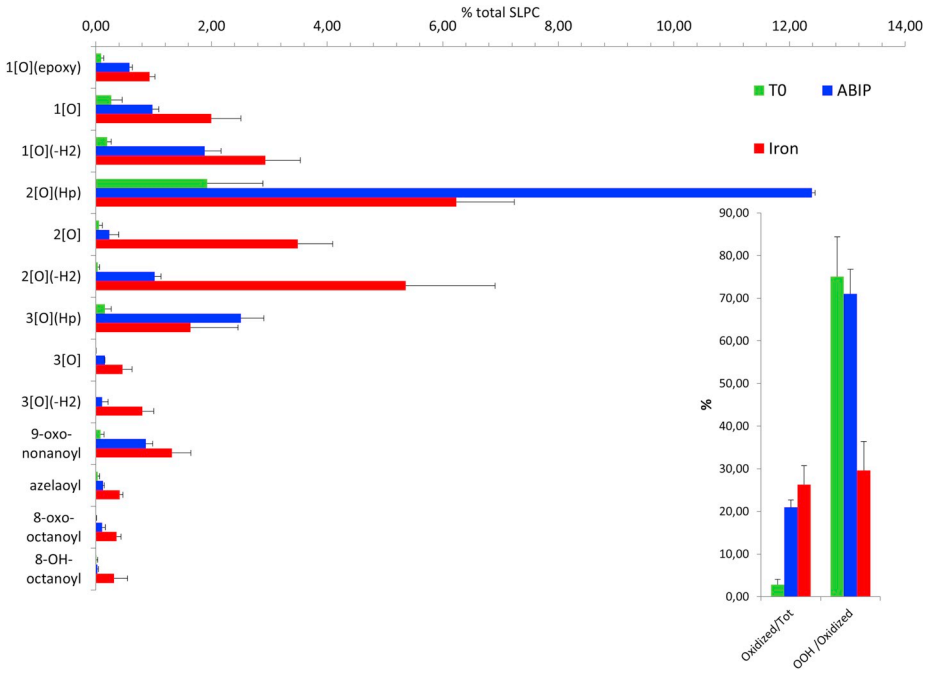

Fig. 2. Lipid oxidation pattern induced by diazo compounds or Fe^{2+}/ascorbate. Oxidized lipids pattern, relative to 1-stearoyl-2-linoleoyl-*sn*-glycero-3-phosphocoline (SLPC), of a fresh liposome suspension containing 0.1 mM phospholipids (SLPC:SLPE/1:1), was measured at time 0 (T_0) and after 30 min of incubation with ABIP 8 mM or Fe^{2+} 4 μM plus Ascorbate 30 μM. In the inset are summarized the percentage of the overall oxidized species versus total amount of SPLC (left) and the percentage of lipo-hydroperoxides versus the sum of oxidized species (right). Values represent the mean ± standard deviation of 20 independent experiments.

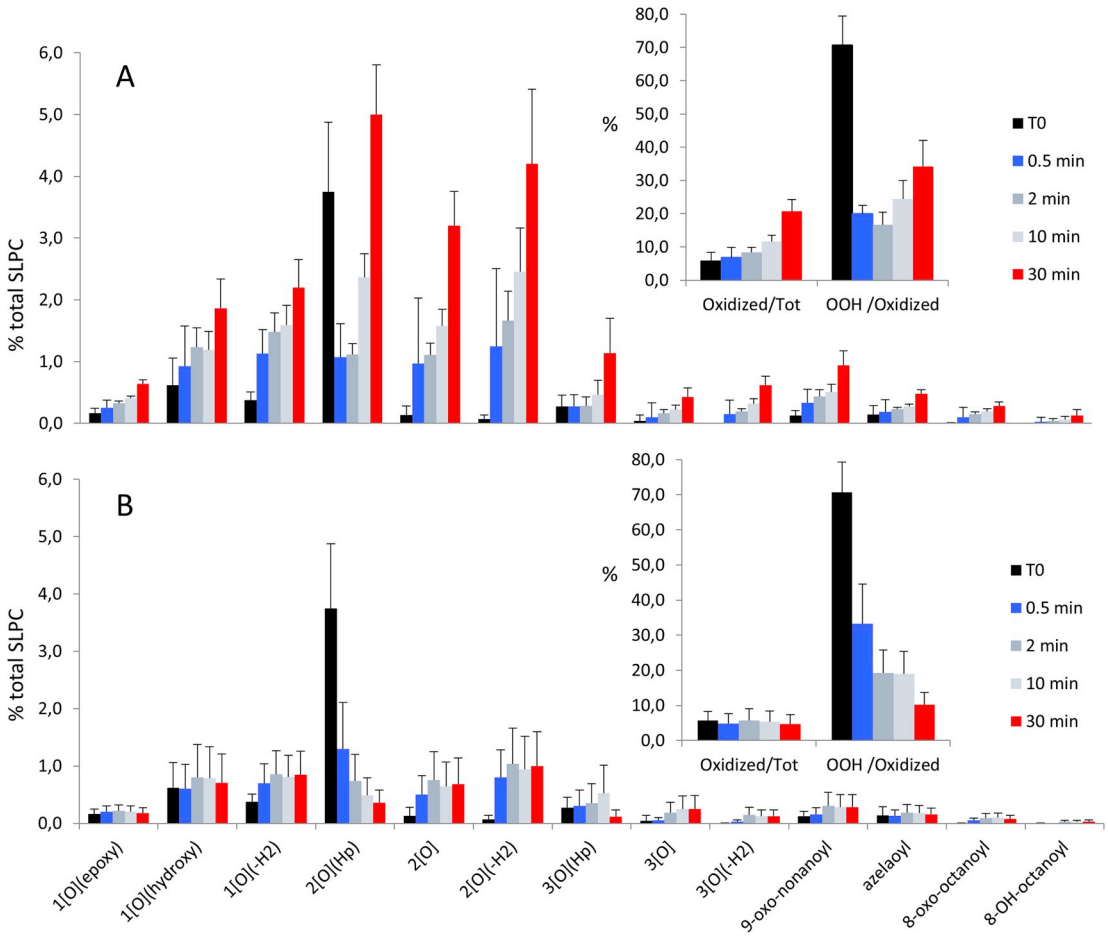

Fig. 3. Time course of Fe^{2+} induced SLPC oxidation pattern, and fer-1 effect. Liposomes suspension, containing 0.1 mM phospholipids (SLPC:SLPE/1:1), was incubated for 30 min with Fe^{2+} 4 μM and Ascorbate 30 μM in absence (A) or in presence (B) of 0.5 μM fer-1. Samples were withdrawn before additions (T_0) and at 0.5, 2, 10, 30 min after additions. In the insets the percentage of the overall oxidized species versus total amount of SPLC (left) and the percentage of lipo-hydroperoxides versus the sum of oxidized species (right) are summarized. Values represent the mean ± standard deviation of 3 independent experiments.

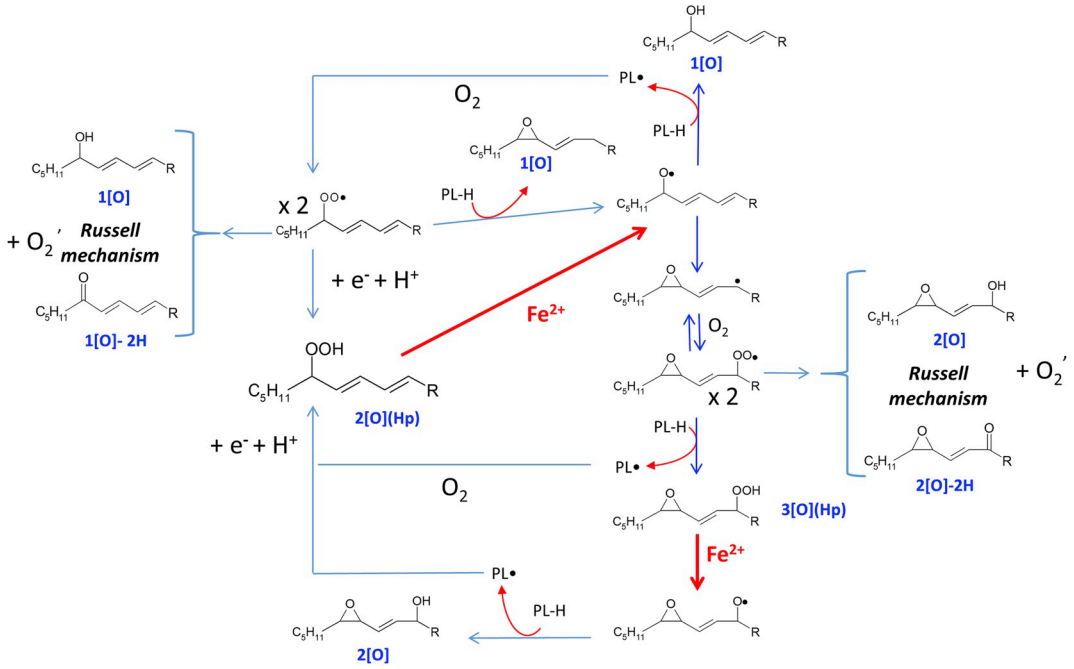

Fig. 4. Schematic outline of Fe^{2+} induced lipid peroxidation mechanism.

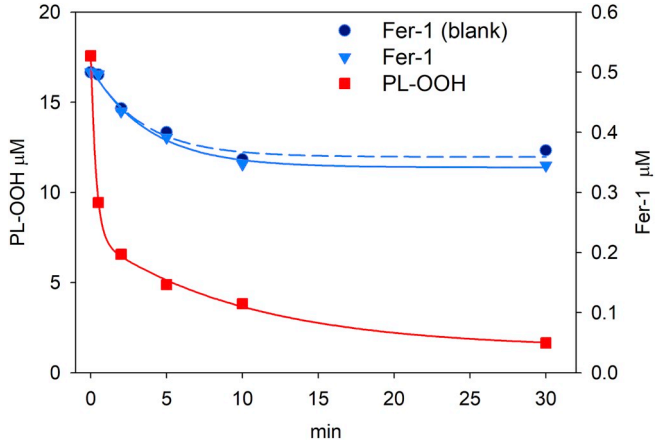

Fig. 5. Lipid hydroperoxide decomposition and fer-1 consumption in the presence of iron. A solution containing 0.1 mM phospholipids (SLPC:SLPE/1:1) in 0.1 M Tris, 0.15 M KCl at pH 7.4, enriched with hydroperoxides by a pretreatment with Alox15 for 60min, was treated with 0.5 µM fer-1, 30 µM ascorbic acid and 4 µM $FeSO_4$, at 37 °C. Time course of total PL-OOH (square ■) and fer-1 (triangle▼) were quantified by Mass Spectrometry. Blank was fer-1 in buffer (circle ●).

3. Results

3.1. Ferrostatin-1 and trolox, have a markedly different lipid peroxidation inhibition efficiency, while sharing the same chain breaking antioxidant effect

We compared the antioxidant capacity of trolox and fer-1 using: i) a diazo compound generating lipid hydroperoxyl radicals; and ii) ferrous iron - ascorbate initiating peroxidation from traces of lipid hydroperoxides present in liposomes. The extruded liposome dispersion containing 0.1 mM phospholipids (SLPC 18:0/18:2 and SLPE 18:0/18:2, ratio 1:1), was introduced in an oxygraphic cell and equilibrated with air in the presence of either fer-1 or trolox. Peroxidation was initiated by adding: ABIP or $FeSO_4$ – ascorbic acid (see Materials and Methods for details). The dependence of initial oxygen consumption rate in the absence and in the presence of trolox or fer-1 concentrations was calculated (see Materials and Methods).

Results reported in Fig. 1 A clearly show that fer-1 and trolox have the same chain-breaking capacity in the presence of ABIP (IC_{50} = 1.66 µM and 1.86 µM, respectively, Fig. 1C). Fer-1 was, instead, much more efficient than trolox when peroxidation was initiated by Fe^{2+} (IC_{50} = 0.017 µM and 7.2 µM, respectively, Fig. 1B and C).

The result supports the conclusion that the efficiency of scavenging of lipid hydroperoxyl radicals does not reflect the antiperoxidant capacity in a model mimicking lipid peroxidation, taking place in FTP.

3.2. Lipidomic analysis of lipid oxidation products

For these experiments we used extruded unilamellar liposomes containing SLPC, SLPE, PLPC, PLPE. The liposome dispersions contained 100 µM phospholipids at 1:1 ratio SLPC:SLPE or PLPC:PLPE.

Approximately 1% of hydroperoxide derivative of linoleic acid generated by autoxidation and trace amount of all other peroxidized species (see below) were present in the phospholipid preparations. Lipid peroxidation was induced by either 8 mM ABIP or 0.1 µM $FeSO_4$-30 µM Ascorbate and recorded for 30 min. Lipids were extracted by a one-phase extraction procedure and analyzed by HPLC-MS/MS.

In a series of preliminary experiments, we confirmed the assumption that only peroxidation products of linoleic acid are generated and that the pattern is the same in different phospholipid species. As expected, indeed, the presence of stearic or palmitic acid as well as the polar head, choline or ethanolamine, does not affect the final pattern of oxidation products of linoleate bound to the phospholipid inserted in the bilayer. Thus, for sake of simplicity we report only results generated from SLPC.

The identification was based on MS/MS spectra, integrated with retention time. As basic reference compounds, we used hydroperoxides produced by ALOX 15 and reduced by GPx4-GSH. The list of most relevant (> 0.1%) oxidized species detected is reported in Table 1.

The pattern of lipid peroxidation products is quite different when liposomes are peroxidized either by the diazo compound or Fe^{2+}. When, after 30 min, approximately 20% of the phospholipids are oxidatively modified, hydroperoxides account for 70% of oxidized species generated by the diazo compound, whilst no more than 30% when

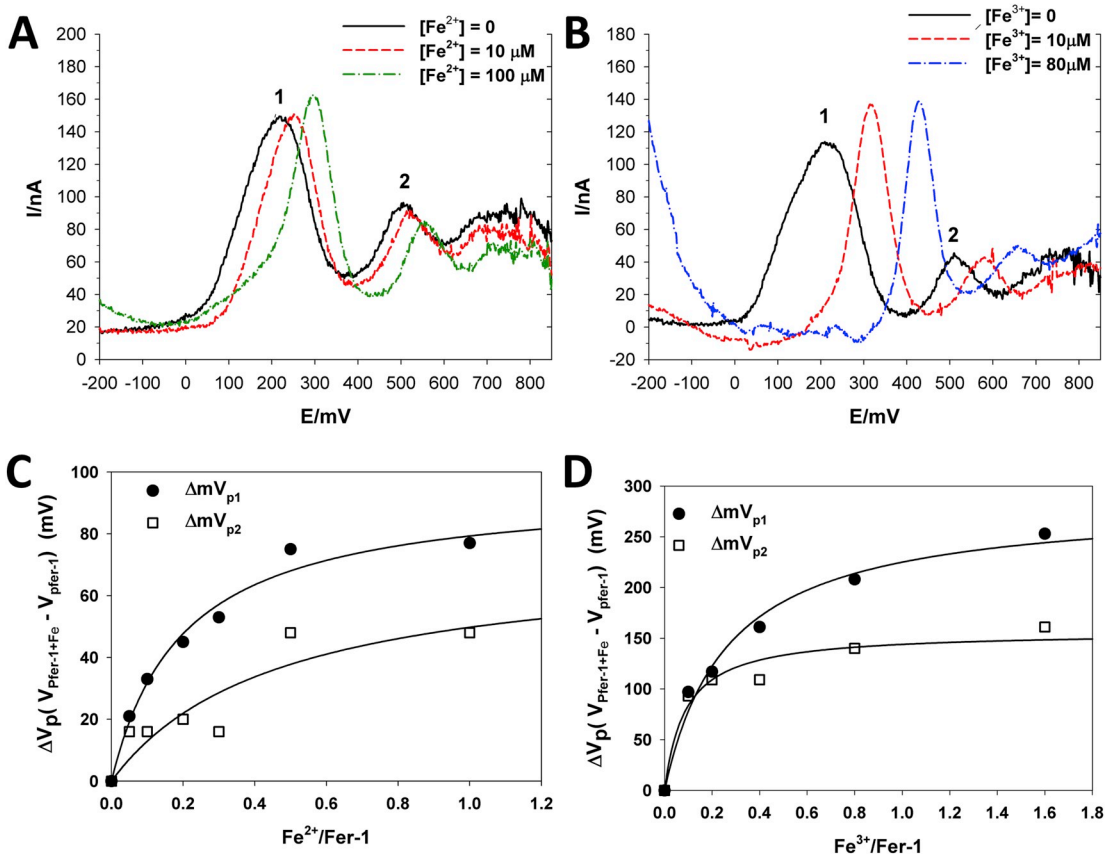

Fig. 6. Effect of ferric and ferrous ions on the anodic peak potential values of fer-1. Differential pulse voltammograms of fer-1 in the absence and presence of different ferrous (A) and ferric (B) ion concentrations show the anodic shift of peak potential values of fer-1 induced by iron. Plots of the shifts of the peak potentials ($\Delta Vp = Vp_{Fer\text{-}1+Fe} - Vp_{Fer\text{-}1}$) on the Fe^{2+}/fer-1 (C) and Fe^{3+}/fer-1 (D) are shown; continuous lines are the results of the best fitting of the hyperbola equation for the experimental data, by non-linear regression analysis.

peroxidation is primed by iron (Fig. 2).

The pattern of lipid peroxidation products, produced by the diazo initiator, complies with the acknowledged mechanism where lipid hydroperoxyl radicals evolve to lipid hydroperoxides and minor species generated by radical-radical interaction leading to termination of the peroxidation chain. In this model of lipid peroxidation, where the lipid hydroperoxyl radical is the peroxidation driving species, the scavenging capacity of chromanol ring (trolox) is similar to that of fer-1 (see Fig. 1 A).

When peroxidation is initiated by Fe^{2+}, lipid hydroperoxides are still the major lipid peroxidation product after 30 min but also substantial amounts of epoxy-keto, epoxy-hydroxy, keto, hydroxy, epoxy-hydroperoxy are produced. The time course of Fe^{2+} induced lipid peroxidation (Fig. 3A) shows the progressive increase of all peroxidation products, while lipid hydroperoxides initially present in the liposome preparation (t = 0) suddenly decrease upon the exposure to Fe^{2+} and then progressively increase. The result fully complies with the proposed mechanism of initiation of lipid peroxidation by lipid alkoxyl radical.

The schematic outline (Fig. 4) of the mechanism complying with our experimental evidence (Fig. 3A) is in agreement with acknowledged mechanisms reviewed in Refs. [17,18].

In summary (for acronym see also Table 1):

1) From lipid hydroperoxides, 2[O](Hp), Fe^{2+} generates lipid alkoxyl radicals PL-O$^{\bullet}$ [38];
2) PL-O$^{\bullet}$ evolves to: i) the hydroxy 1[O] generating new lipid carbon center radical, PL$^{\bullet}$, that reversibly adds oxygen and forms PL-OO$^{\bullet}$, in turn stabilized as hydroperoxide 2[O](Hp) by H transfer; ii) the epoxy-allylic carbon centered radical, Ep-PL$^{\bullet}$, [39] that also adds oxygen forming Ep-PL-OO$^{\bullet}$ stabilized as hydroperoxide, 3[O](Hp), by H transfer.
3) PL-OO$^{\bullet}$ and Ep-PL-OO$^{\bullet}$ may dismutate via Russell mechanism [40] producing singlet oxygen and 1[O] plus 1[O]-H2 from PL-OO$^{\bullet}$ and 2[O] plus 2[O]-H2 from Ep-PL-OO$^{\bullet}$.
4) PL-OO$^{\bullet}$ (and Ep-PL-OO$^{\bullet}$) may also react with LH with the formation of another alkoxyl radical PL-O$^{\bullet}$ [41] and the epoxy 1[O] (isobaric with the hydroxy species).
5) From 3[O](Hp), Fe^{2+} generates an epoxy alkoxyl radicals Ep-PL-O$^{\bullet}$ in turn evolving similarly to PL-O$^{\bullet}$ and initiating a new chain reaction.

Different oxygenated radical species may also generate truncated phospholipids and small molecular weight compounds that, being produced in minimal amount, have not been further investigated for the specific purpose of this study.

When iron dependent lipid peroxidation is inhibited by fer-1 (Fig. 3B), the lipid hydroperoxides present in liposomes disappear giving rise to the series of oxidized species the pattern of which is identical to that observed when peroxidation is not inhibited (Fig. 3A). This evidence is in agreement with the notion that the most relevant reaction of fer-1 is scavenging of the PL-O$^{\bullet}$ competent for initiating lipid peroxidation.

Instead, the scavenging of a PL-OO$^{\bullet}$, i.e. the chain breaking effect, competes with propagation, but also stabilizes the reversible oxygen addition generating a new hydroperoxide from which iron initiates new peroxidative chain reactions.

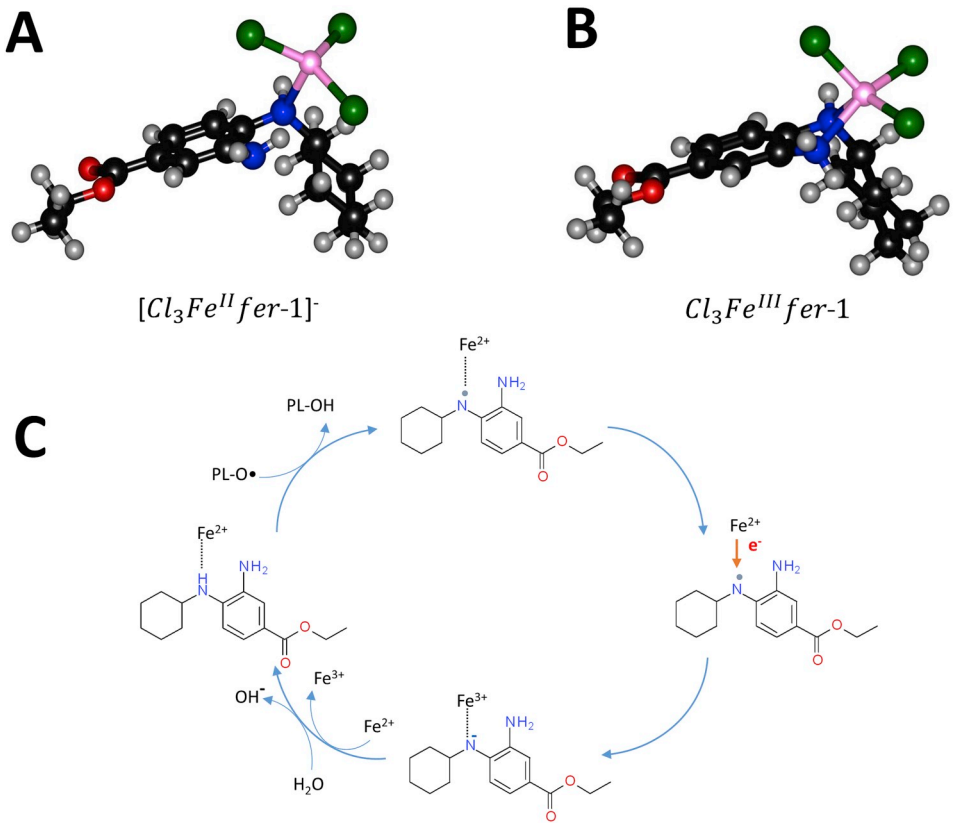

Fig. 7. Molecular structures of iron complexes with ferrostatin-1 fully optimized at M06-L/6–31G(d,p), LanL2DZ level of theory. Fer-1/Fe^{II} (A) and fer-1/Fe^{III} (B) complexes are shown in (A) and (B) respectively. In (C) a schematic view of fer-1 scavenging the lipid alkoxy radicals (PL-O·) and reduction of fer-1 radical by ferrous iron is depicted.

$$\left[Cl_3Fe^{II}fer1\right]^- + CH_3OO\cdot \rightarrow [Cl_3Fe^{II}fer1(-H)]\cdot^- + CH_3OOH$$

$$[Cl_3Fe^{II}fer1(-H)]\cdot^- \rightarrow [Cl_3Fe^{III}fer1(-H)]^-$$

$$[Cl_3Fe^{III}fer1(-H)]^- + H_2O \rightarrow [Cl_3Fe^{III}fer1] + OH^-$$

Scheme 1. Elementary steps of radical reduction via HAT from fer-1.

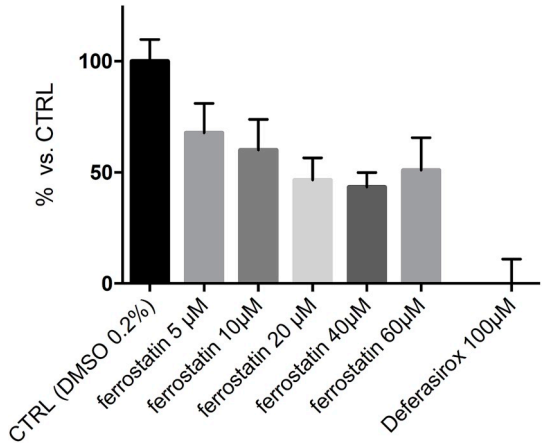

Fig. 8. Fer-1 binds iron of Labile Iron Pool (LIP). Relative LIP was expressed as calcein Mean Fluorescence Intensity (MFI) in treated cells *vs.* control. Cells incubated with Deferasirox 100 μM served as baseline. The values are the mean ± standard deviation (SD) of 2 experiment in triplicate.

3.3. Ferrostatin-1 inhibits peroxidation without being consumed

Surprisingly, we observed that fer-1 is not consumed while inhibiting iron induced peroxidation. This remarkable evidence is exemplified in Fig. 5 where it is reported that 0.5 μM fer-1 is not consumed during iron driven hydroperoxide decomposition, even in the presence of 15 μM lipid hydroperoxides (Fig. 5). It is worth to note that, the superstoichiometric efficiency of fer-1 has been previously reported for diarylamines although in a deeply different experimental condition [42]. Conversely, when peroxidation was induced by the diazo compound, fer-1 disappears (see Supplementary Material table S1), seemingly forming products that have not been further investigated.

These results stimulated the hypothesis that the radical of fer-1 produced by the interaction with the alkoxyl radical, could be reduced back. Compelling evidence suggested the hypothesis that it is ferrous iron itself the electron donor in this reaction. The hypothesis was tested seeking for evidence, firstly for the interaction of fer-1 with iron by electroanalytical measurements and then by quantum-mechanics calculations of the energetics of the redox process. Secondly, the formation of a complex between fer-1 and iron was demonstrated in cells by fluorescence of calcein.

3.4. Electroanalytical analysis of the interaction between fer-1 and iron

Differential pulse voltammetry (DPV) measurements were performed in methanol 90% and $LiClO_4$ buffer (0.1 M). Fe^{2+} or Fe^{3+} was stepwise added (from 10 to 100 μM, final concentration) to 100 μM fer-1, and the generated current recorded. Both the oxidation peaks of fer-1 were shifted towards more positive potentials (anodic shift) in the presence of iron (Fig. 6 A and B). These shifts of the peak potentials ($\Delta Vp = Vp_{Fer\text{-}1+Fe} - Vp_{Fer\text{-}1}$) dependent on the fer-1/Fe ratio, fulfilled the expected saturation kinetics (Fig. 6C and D). The hyperbola equation was found to fit well the experimental data.

The best fitting indicates that maxima were reached at approximately the value of 1 for both Fe^{2+}/fer-1 and Fe^{3+}/fer-1, indicating that a saturation is reached at a fer-1:iron ratio, about 1:1. These results support the notion that iron interacts with fer-1, forming a complex, as already reported for other antioxidants or complexing molecules [36].

3.5. Hydrogen Atom Transfer (HAT) mechanism in ferrostatin-1

The DFT analysis indicates that fer-1 can bind to iron through the N lone pairs. In our model, the coordination sphere is saturated by three Cl anions, so that the overall molecular charge is -1. Notably, since only the secondary amine N binds to iron, the complex is tetracoordinated (Fig. 7A). Its electronic ground state is a quintet, characterized by four electrons with parallel spin on the metal center. The electronic structure, computed in gas-phase at M06-L/6-311 + G(d,p),LanL2DZ//M06-L/6-31G(d,p),Lan2DZ level of theory, is consistent with this, since a Mulliken spin density value of 3.69 is obtained for the iron nucleus. This complex can reduce radicals via HAT (Hydrogen Atom Transfer) mechanism. We have considered the primary and the secondary amines as the most reactive sites of the fer-1, by analogy with the free fer-1 and similar organic systems [43,44]. Initially, a radical complex is formed, with four unpaired electrons on iron and one unpaired electron on N, in which iron maintains the initial oxidation state.

In the computational analysis, we used $CH3O^{\bullet}$ and $CH3OO^{\bullet}$ as models of lipid alkoxyl and hydroperoxyl radicals (PL-$O^{\bullet}$ and PL-$OO^{\bullet}$), respectively. The radical formation on the secondary amine N site is more stable by 23.2 kcal mol^{-1} (value computed in gas phase) than on the primary amine N site. Afterwards, through an intramolecular electron transfer, iron(II) is oxidized to iron(III) and the N atom becomes negatively charged. In this complex, the overall multiplicity is a sextet and the five unpaired electrons are localized on the iron center. Fer-1 is subsequently protonated upon reaction with a water molecule, forming the penta-coordinated complex (Fig. 7B); the Mulliken spin density on iron is 3.92, but when considering the three Cl atoms the total value is 4.84. In Scheme 1, the three steps above described are summarized.

By combining the three reactions of Scheme 1, we can write the overall process (Eq. (2)), as well as the same process in presence of the alkoxyl radical (Eq. (3)):

$$[Cl_3Fe^{II}fer-1]^- + CH_3OO^{\cdot} + H_2O \rightarrow [Cl_3Fe^{III}fer-1] + OH^- + CH_3OOH \quad (2)$$

$$[Cl_3Fe^{II}fer-1]^- + CH_3O^{\cdot} + H_2O \rightarrow [Cl_3Fe^{III}fer-1] + OH^- + CH_3OH \quad (3)$$

The Gibbs free reaction energies, representing the thermodynamic force driving the overall process of radical reduction by HAT from fer-1, computed in benzene and water, to mimic an apolar and a polar environment, respectively, are 48.3 and 10.9 kcal mol^{-1} referring to $CH_3OO^{\bullet}$ radical and 28.3 and -9.1 kcal mol^{-1} referring to the $CH_3O^{\bullet}$ radical. This denote the scavenging capacity of fer-1 and its preference for alkoxyl rather than hydroperoxyl radical (Fig. 7C).

3.6. Ferrostatin-1 reduces the labile iron pool in cells

The procedure based on cytochemical calcein-AM (calcein-acetoxymethyl ester) [45] was used to assay the dimension of the cellular 'labile iron pool' (LIP). Increasing concentrations of fer-1 were added to the assays using DMSO as control. To demonstrate the validity of the procedure 100 μM deferasirox was used as positive control. Differently from the iron chelator, which completely abrogates the cellular LIP, 20 μM fer-1 was effective in reducing the labile iron pool concentration by no more than 50% (Fig. 8). This result, together with the evidences obtained through DVP and DFT, supports the notion that fer-1 can interact with at least part of the cellular LIP. This further validates the conclusion that fer-1 forms a complex with iron and indirectly supports the theoretical mechanistic evidence that Fe^{2+} reduces fer-1 radical.

4. Conclusions

Ferroptosis is a recently described, non-apoptotic, iron dependent form of RCD, operated by lipid peroxidation (LPO), and challenged by the "peroxidation inhibiting protein" GPx4. In particular, LPO is initiated by the iron dependent decomposition of the O–O bond in phospholipid hydroperoxides (PL-OOH), thus generating the initiating PL-$O^{\bullet}$. Oxygen addition generates the PL-$OO^{\bullet}$, which propagates the radical reaction in competition with the termination by radical-radical interaction, through the interaction with new PL containing a polyunsaturated fatty acid; this produces another PL-OOH and a new $PL^{\bullet}$. In the last decades, azo initiators were largely used for mechanistic and kinetic studies on LPO. These compounds produce a carbon centered radical evolving to a hydroperoxyl radical and were exploited for the evaluation of the "antioxidant capacity" of natural and synthetic molecules. However, assays using azo compounds, although measuring the "chain breaking" efficiency of the antioxidant, an event representing the inhibition of the propagation step of the chain reaction, cannot be considered fully overlapping with the concept of "free radical scavenging antioxidant". Indeed, in the case of iron dependent lipid peroxidation, the role of initiating PL-$O^{\bullet}$ is critically more relevant, since the propagation step generates new PL-OOH from which Fe^{2+} keeps regenerating initiating radicals, by Fenton like reaction.

Fer-1 is a synthetic compound isolated by high-throughput screening of small molecule libraries as a potent inhibitor of FTP. Although fer-1 acts as a classic hydroperoxyl radical scavenger, this chain breaking mechanism cannot account for the observed inhibition of FTP.

Our results demonstrated that, when fer-1 inhibits peroxidation, initiated by iron and traces of lipid hydroperoxides in liposomes, the pattern of the oxidized products was superimposable to that observed following exhaustive non inhibited lipid peroxidation. This supported the notion that the *anti*-ferroptotic activity of fer-1 is actually due to the scavenging of initiating alkoxyl radicals produced by ferrous iron from lipid hydroperoxides.

Notably, fer-1 acts in a para-catalytic way, being not consumed while inhibiting iron dependent lipid peroxidation. Supported by electroanalytical evidence that fer-1 forms a complex with iron, we propose that it is the ferrous iron itself that reduces fer-1 radical. This mechanism was corroborated by DFT calculations showing: i) the reduction the alkoxyl radical by fer-1; and ii) the reduction of fer-1 radical by ferrous iron. The evidence that in HEK293T cells fer-1 decreases the cell labile iron pool, is consistent with our conclusions.

In summary, fer-1, in the presence of reduced iron, eliminates lipid hydroperoxides, producing the same *anti*-ferroptotic effect as GPx4, although generating a series of oxidized species but not just hydroxy fatty acids derivatives as the enzyme does.

Funding

This work was supported by the Institutional grants from the University of Padova, Italy (COZZ_SID18_01 to G.C. and MIOT_SID17_01 to G.M), by the Human Frontier Science Program Organization (RGP0013/2014) to F.U. and by the ISCRA Grant REBEL2 (REdox state role in Bio-inspired ELementary reactions 2) to L.O.

Acknowledgements

CINECA (Casalecchio di Reno, Italy) is gratefully acknowledged for providing the supercomputing facilities used for the DFT calculations.

Appendix A. Supplementary data

Supplementary data to this article can be found online at https://doi.org/10.1016/j.redox.2019.101328.

References

[1] S.J. Dixon, K.M. Lemberg, M.R. Lamprecht, R. Skouta, E.M. Zaitsev, C.E. Gleason,

et al., Ferroptosis: an iron-dependent form of nonapoptotic cell death, Cell 149 (2012) 1060–1072.
[2] S.J. Guiney, P.A. Adlard, A.I. Bush, D.I. Finkelstein, S. Ayton, Ferroptosis and cell death mechanisms in Parkinson's disease, Neurochem. Int. 104 (2017) 34–48.
[3] M. Conrad, J.P. Angeli, P. Vandenabeele, B.R. Stockwell, Regulated necrosis: disease relevance and therapeutic opportunities, Nat. Rev. Drug Discov. 15 (2016) 348–366.
[4] L. Magtanong, S.J. Dixon, Ferroptosis and brain injury, Dev. Neurosci. (2019) 1–14.
[5] H. Zhu, A. Santo, Z. Jia, Y. Robert Li, GPx4 in Bacterial Infection and Polymicrobial Sepsis: Involvement of Ferroptosis and Pyroptosis, React. Oxyg. Species (Apex) 7 (2019) 154–160.
[6] E.P. Amaral, D.L. Costa, S. Namasivayam, N. Riteau, O. Kamenyeva, L. Mittereder, et al., A major role for ferroptosis in Mycobacterium tuberculosis-induced cell death and tissue necrosis, J. Exp. Med. 216 (2019) 556–570.
[7] A. Bhaskar, M. Munshi, S.Z. Khan, S. Fatima, R. Arya, S. Jameel, et al., Measuring glutathione redox potential of HIV-1-infected macrophages, J. Biol. Chem. 290 (2015) 1020–1038.
[8] M. Maiorino, M. Conrad, F. Ursini, GPx4, lipid peroxidation, and cell death: discoveries, rediscoveries, and open issues, Antioxidants Redox Signal. 29 (2018) 61–74.
[9] F. Ursini, M. Maiorino, M. Valente, L. Ferri, C. Gregolin, Purification from pig liver of a protein which protects liposomes and biomembranes from peroxidative degradation and exhibits glutathione peroxidase activity on phosphatidylcholine hydroperoxides, Biochim. Biophys. Acta 710 (1982) 197–211.
[10] F. Ursini, M. Maiorino, C. Gregolin, The selenoenzyme phospholipid hydroperoxide glutathione peroxidase, Biochim. Biophys. Acta 839 (1985) 62–70.
[11] M. Maiorino, M. Coassin, A. Roveri, F. Ursini, Microsomal lipid peroxidation: effect of vitamin E and its functional interaction with phospholipid hydroperoxide glutathione peroxidase, Lipids 24 (1989) 721–726.
[12] W.A. Pryor, first ed., Free Radicals in Biology vol. I, Academic Press, New York, 1976.
[13] H. Kuhn, S. Banthiya, K. van Leyen, Mammalian lipoxygenases and their biological relevance, Biochim. Biophys. Acta Mol. Cell Biol. Lipids 1851 (2015) 308–330.
[14] L.F. Ye, B.R. Stockwell, Transforming lipoxygenases: PE-specific enzymes in disguise, Cell 171 (2017) 501–502.
[15] K. Schnurr, J. Belkner, F. Ursini, T. Schewe, H. Kuhn, The selenoenzyme phospholipid hydroperoxide glutathione peroxidase controls the activity of the 15-lipoxygenase with complex substrates and preserves the specificity of the oxygenation products, J. Biol. Chem. 271 (1996) 4653–4658.
[16] B. Maillard, K.U. Ingold, J.C. Scaiano, Rate constants for the reactions of free radicals with oxygen in solution, J. Am. Chem. Soc. 105 (1983) 5095–5099.
[17] H. Yin, L. Xu, N.A. Porter, Free radical lipid peroxidation: mechanisms and analysis, Chem. Rev. 111 (2011) 5944–5972.
[18] Z.Y. Cheng, Y.Z. Li, What is responsible for the initiating chemistry of iron-mediated lipid peroxidation: an update, Chem. Rev. 107 (2007) 748–766.
[19] K.U. Ingold, T. Paul, M.J. Young, L. Doiron, Invention of the first azo compound to serve as a superoxide thermal source under physiological conditions: concept, synthesis, and chemical properties, J. Am. Chem. Soc. 119 (1997) 12364–12365.
[20] S.M. Culbertson, N.A. Porter, Design of unsymmetrical azo initiators to increase radical generation efficiency in low-density lipoproteins, Free Radic. Res. 33 (2000) 705–718.
[21] F. Ursini, I. Rapuzzi, R. Toniolo, F. Tubaro, G. Bontempelli, Characterization of antioxidant effect of procyanidins, Methods Enzymol. 335 (2001) 338–350.
[22] J.P. Friedmann Angeli, M. Schneider, B. Proneth, Y.Y. Tyurina, V.A. Tyurin, V.J. Hammond, et al., Inactivation of the ferroptosis regulator Gpx4 triggers acute renal failure in mice, Nat. Cell Biol. 16 (2014) 1180–1191.
[23] R. Skouta, S.J. Dixon, J. Wang, D.E. Dunn, M. Orman, K. Shimada, et al., Ferrostatins inhibit oxidative lipid damage and cell death in diverse disease models, J. Am. Chem. Soc. 136 (2014) 4551–4556.
[24] O. Zilka, R. Shah, B. Li, J.P. Friedmann Angeli, M. Griesser, M. Conrad, et al., On the mechanism of cytoprotection by ferrostatin-1 and liproxstatin-1 and the role of lipid peroxidation in ferroptotic cell death, ACS Cent. Sci. 3 (2017) 232–243.
[25] A. Roveri, M. Maiorino, C. Nisii, F. Ursini, Purification and characterization of phospholipid hydroperoxide glutathione peroxidase from rat testis mitochondrial membranes, Biochim. Biophys. Acta 1208 (1994) 211–221.
[26] T. Horn, I. Ivanov, A. Di Venere, K.R. Kakularam, P. Reddanna, M.L. Conrad, et al., Molecular basis for the catalytic inactivity of a naturally occurring near-null variant of human ALOX15, Biochim. Biophys. Acta 1831 (2013) 1702–1713.
[27] G. Cozza, M. Rossetto, V. Bosello-Travain, M. Maiorino, A. Roveri, S. Toppo, et al., Glutathione peroxidase 4-catalyzed reduction of lipid hydroperoxides in membranes: the polar head of membrane phospholipids binds the enzyme and addresses the fatty acid hydroperoxide group toward the redox center, Free Radic. Biol. Med. 112 (2017) 1–11.
[28] D.D. Wayner, G.W. Burton, K.U. Ingold, S. Locke, Quantitative measurement of the total, peroxyl radical-trapping antioxidant capability of human blood plasma by controlled peroxidation. The important contribution made by plasma proteins, FEBS Lett. 187 (1985) 33–37.
[29] A. Rigo, F. Vianello, G. Clementi, M. Rossetto, M. Scarpa, U. Vrhovsek, et al., Contribution of proanthocyanidins to the peroxy radical scavenging capacity of some Italian red wines, J. Agric. Food Chem. 48 (2000) 1996–2002.
[30] R.M. Pellegrino, A. Di Veroli, A. Valeri, L. Goracci, G. Cruciani, LC/MS lipid profiling from human serum: a new method for global lipid extraction, Anal. Bioanal. Chem. 406 (2014) 7937–7948.
[31] L. Goracci, S. Tortorella, P. Tiberi, R.M. Pellegrino, A. Di Veroli, A. Valeri, et al., Lipostar, a comprehensive platform-neutral cheminformatics tool for lipidomics, Anal. Chem. 89 (2017) 6257–6264.
[32] Frisch MJ, Trucks GW, Schlegel HB, Scuseria GE, Robb MA, Cheeseman JR, et al Gaussian 16 Rev. B.01. Wallingford, CT2016.
[33] Y. Zhao, D.G. Truhlar, The M06 suite of density functionals for main group thermochemistry, thermochemical kinetics, noncovalent interactions, excited states, and transition elements: two new functionals and systematic testing of four M06-class functionals and 12 other functionals, Theor. Chem. Acc. 120 (2008) 215–241.
[34] A.V. Marenich, C.J. Cramer, D.G. Truhlar, Universal solvation model based on solute electron density and on a continuum model of the solvent defined by the bulk dielectric constant and atomic surface tensions, J. Phys. Chem. B 113 (2009) 6378–6396.
[35] M. Bortoli, M. Dalla Tiezza, C. Muraro, C. Pavan, G. Ribaudo, A. Rodighiero, et al., Psychiatric disorders and oxidative injury: antioxidant effects of zolpidem therapy disclosed in silico, Comput. Struct. Biotechnol. J. 17 (2019) 311–318.
[36] V. Chobot, F. Hadacek, W. Weckwerth, L. Kubicova, Iron chelation and redox chemistry of anthranilic acid and 3-hydroxyanthranilic acid: a comparison of two structurally related kynurenine pathway metabolites to obtain improved insights into their potential role in neurological disease development, J. Organomet. Chem. 782 (2015) 103–110.
[37] M. Salas-Reyes, J. Hernandez, Z. Dominguez, F.J. Gonzalez, P.D. Astudillo, R.E. Navarro, et al., Electrochemical oxidation of caffeic and ferulic acid derivatives in aprotic medium, J. Braz. Chem. Soc. 22 (2011) 693-U346.
[38] B. Halliwell, J.M.C. Gutteridge, Free Radicals in Biology and Medicine, Clarendon Press, Oxford, 1986.
[39] L. Grossi, S. Strazzari, B.C. Gilbert, A.C. Whitwood, Oxiranylcarbinyl radicals from allyloxyl radical cyclization: characterization and kinetic information via ESR spectroscopy, J. Org. Chem. 63 (1998) 8366–8372.
[40] G.A. Russell, Deuterium-isotope effects in the autoxidation of aralkyl hydrocarbons. Mechanism of the interaction of peroxy radicals, J. Am. Chem. Soc. 79 (1957) 3871–3877.
[41] T. Aliwarga, B.S. Raccor, R.N. Lemaitre, N. Sotoodehnia, S.A. Gharib, L. Xu, et al., Enzymatic and free radical formation of cis- and trans- epoxyeicosatrienoic acids in vitro and in vivo, Free Radic. Biol. Med. 112 (2017) 131–140.
[42] E.A. Haidasz, R. Shah, D.A. Pratt, The catalytic mechanism of diarylamine radical-trapping antioxidants, J. Am. Chem. Soc. 136 (2014) 16643–16650.
[43] X. Sheng, C. Shan, J. Liu, J. Yang, B. Sun, D. Chen, Theoretical insights into the mechanism of ferroptosis suppression via inactivation of a lipid peroxide radical by liproxstatin-1, Phys. Chem. Chem. Phys. 19 (2017) 13153–13159.
[44] X.H. Sheng, C.C. Cui, C. Shan, Y.Z. Li, D.H. Sheng, B. Sun, et al., O-Phenylenediamine: a privileged pharmacophore of ferrostatins for radical-trapping reactivity in blocking ferroptosis, Org. Biomol. Chem. 16 (2018) 3952–3960.
[45] W. Breuer, S. Epsztejn, Z.I. Cabantchik, Iron acquired from transferrin by K562 cells is delivered into a cytoplasmic pool of chelatable iron(II), J. Biol. Chem. 270 (1995) 24209–24215.